 doi:10.20944/preprints202002.0457.v1

Influence of Cross Section Thickness and Aspect Ratio on Deformation during Diffusion Bonding and Impact of Metal Diffusion and Evaporation on Temperature Measurement Accuracy

Thomas Gietzelt, Volker Toth, Manfred Kraut, U. Gerhards, R. Dürrschnabel*

[*] *Dr. Thomas Gietzelt, KIT, Institute of Micro Process Engineering*

PoBox 3640, 76021 Karlsruhe

thomas.gietzelt@kit.edu

Abstract:

Diffusion bonding is often used on pre-machined parts to generate internal cavities, e.g. for cooling injection molding tools close to the mold cavity. Only then, the workpieces are finished to their final dimensions. In the case of micro-process devices, however, it is essential to precisely control the deformation, as otherwise uncontrollable pressure losses will occur with channel cross-sections in the sub-millimeter range. Post-processing is not possible.

The most important process parameters for diffusion bonding are temperature, dwell time and contact pressure, with the bonding temperature and contact pressure acting in opposite directions and showing a strong non-linear dependence on deformation. In addition, the deformation is influenced by a number of other factors such as the absolute size of the cross-section and the aspect ratio of the parts, the dimensions and distribution of the internal cross sections and the overall percentage of the cross-section to be bonded.

In micro process engineering, small material cross-sections in the range of the materials microstructure can facilitate additional deformation mechanisms such as grain boundary sliding, which are not relevant at all for larger structures.

For parts consisting of multiple layers, tolerances in thickness and roughness of multiple surfaces must be levelled, contributing to the percentaged deformation. This makes it difficult, especially in micro process engineering and in single or small series production, to determine

 doi:10.20944/preprints202002.0457.v1

suitable joining parameters in advance, which on the one hand do not cause unforeseen large deformations, but on the other hand reliably produce highly vacuum-tight components.

Hence, a definition of a fixed percentaged deformation does not work for all kinds of components. This makes it difficult to specify parameters for surely obtain high-vacuum tight parts.

For successful diffusion bonding, atoms must diffuse over the bonding planes, forming a monolithic part in which the original layers are no longer visible. Only then, mechanical properties identical to those of the base material, which has been subjected to identical heat treatment, can be achieved.

In this paper, the impacts of different material cross section widths as well as of the aspect ratio on deformation were investigated. By accident, it was found that also accuracy of the temperature measurement may have a serious impact in terms of deformation.

Keywords: diffusion welding, diffusion bonding, cross section width, aspect ratio, material thickness, thermocouple aging

1 Introduction

Diffusion welding is often used to create complex buried structures and channels in components. In mechanical engineering, dimensions in the range of some tenth of a millimeter are relevant. Typically, it is not necessary to control the deformation very exactly. Instead, only the functionality must be guaranteed, e.g. with cooling structures close to the mold cavity. Furthermore, for massive parts such as injection molding tools, the deformation responds not very sensitive to bonding parameters, and these parts are only finished to their final dimensions afterward bonding. The joints are of interest with regard to existence of remaining pores and watertightness only.

 doi:10.20944/preprints202002.0457.v1

Therefore, there is hardly any literature dedicated to deformation control during diffusion bonding. In micro-process engineering, however, the mechanical dimensions are in the sub-millimeter range and thus in the order of magnitude of the materials microstructure. In addition, such devices are usually composed of a large number of microstructured thin layers. There is no continuous joining surface, but only a fraction of the cross-section of the material is passing through the component over its entire height. Due to the small dimension of these columns, deformation mechanisms such as grain boundary gliding may occur, which do not contribute to the deformation for larger components and cross sections. Additionally, for micro process devices, depending on the design, the joining cross section may vary from layer to layer and the question of force transmission, force distribution over several layers and achieving a reproducible joining result over the whole part, occurs. [1]

As the number of layers and the component overall cross section increases, also tolerance considerations applies. Since the variation of the thickness of cold rolled sheet material is in the range of 20-50 µm, it cannot be neglected. [2] With increasing lateral dimensions, manufacturing tolerances may add up or are balanced, causing a poor reproducibility for diffusion bonding of parts of identical design and subjected to the same bonding parameters, in terms of vacuum tightness and percentaged deformation. In practice, locally a much higher contact pressure may apply at the beginning, responsible for increased local deformation and blocking of internal microstructures, before the whole cross section is subjected to an uniform contact pressure. For relatively thin components with a large cross-section, which contain complex internal structures such as constrictions lying one behind the other, the pressure drop for different batches of diffusion-bonded parts may vary greatly and exceed the limits of technical specification.

Beside tolerance considerations of sheet thickness, for multilayered parts, many surface roughnesses must be leveled to make contact at atomic scale. Surprisingly, in the literature only little attention is paid to levelling multiple surface roughnesses of multilayered devices and its

 doi:10.20944/preprints202002.0457.v1

impact on deformation. Unfortunately, the deformation depends on many other parameters too, such as the design, e.g. aspect ratio and width of the cross sections to be joined. Hence, the specification of a percentaged deformation for multilayered devices may not be a suitable criterion to guarantee vacuum-tightness.

In [3], we examined the influence of the number of layers per construction height in comparison to components made of two pieces only as well as the impact of overall cross section and aspect ratio on deformation. However, the roughness values of surfaces were not characterized. In [4], *Zhang* et al. investigated the deformation behavior of asperities during diffusion bonding of milled surfaces possessing a surface roughness R_a=1.6 µm at T=1080°C, t= 20 min and varying contact pressures of 5, 10, 15 and 20 MPa, respectively, in terms of remaining pores. However, unfortunately, different roughness values were not investigated and compared. In [5], we investigated the depth of singular scratches on vacuum tightness and compared the impact of a constant contact pressure to a contact pressure superimposed by short peak loads. However, the influence of the absolute width of joining cross sections on the deformation behavior has not yet been investigated systematically.

In addition to all the parameters mentioned above, the composition of the material has an impact on diffusion and formation of passivation layers, affecting deformation, grain growth across the bonding planes and diffusion bonding result. Therefore, a certain bonding temperature, bonding time and contact pressure do not lead to a reproducible deformation for different parts and materials.

In this paper, test parts possessing a constant bonding area but different dimensional width of material at constant height were investigated. For comparison reasons, three samples with an aspect ratio of about three were bonded for comparison reasons.

During the experiments, it became clear that also inaccuracies in temperature measurement in particular can be responsible for very different deformation values. The reason is that the diffusion coefficient changes strongly non-linearly in the considered temperature range.

Preprints (www.preprints.org) | NOT PEER-REVIEWED | Posted: 29 February 2020 doi:10.20944/preprints202002.0457.v1

2 Materials and Design of Experiments

As material, austenitic stainless steel 1.4301 (AISI 304) with a sheet thickness of 2 mm was used.

To investigate the influence of the lateral dimension independent of the bonding cross-section, a set of samples with a constant cross-section of 5026.6 mm², corresponding to a diameter of 80 mm, were used. In order to save material, overlapping annular test specimens were designed for this purpose (Tab. 1).

Tab. 1: Calculated design of annular test samples consisting of ten layers.

Sample	**d_i [mm]**	**d_o [mm]**	**Cross Section [mm²]**	**Width [mm]**	**Percentaged Mat. Width related to 80 mm [%]**	**Reduction of Mat. Width related to previous Sample by [%]**	**Aspect Ratio**
Diameter		**80**	5026.6		≙100	≙100	0.25
Annular 1	80	113.14	5026.6	16.57	20.25	73.9	1.21
Annular 2	115	140.09	5026.6	12.54	15.50	24.3	1.59
Annular 3	150	170.00	5026.6	10.00	12.38	20.3	2.00
Annular 4	185	201.56	5026.6	8.28	10.13	17.2	2.42
Annular 5	220	234.09	5026.6	7.05	8.63	14.9	2.84
Annular 6	255	267.25	5026.6	6.13	7.43	13.1	3.26

All test specimens were cut by laser out of 1.4301 sheet material, 2 mm in nominal thickness. For this, a *TruLaser Cell 3010*, combined with a 3 kW *TruDisk 3001* by *Trumpf* was used. Due to tolerances arising from laser cutting process, all dimension were checked using a caliper gauge with a scale division of 1/100 mm. From this, the true cross section was calculated, using

Preprints (www.preprints.org) | NOT PEER-REVIEWED | Posted: 29 February 2020 doi:10.20944/preprints202002.0457.v1

the measured width of the annular test samples and the outer diameter. The percentage deviations to 5026.6 mm² were calculated (Tab. 2). It turned out that the error is between -0.25 and -3.16 % due to manufacturing tolerances. This reflects the problem that the same accuracy in one dimension effects larger errors in area.

For the first set of bonding experiments, ten layers were stacked each, leading to varying aspect ratios (Tab. 1).

Tab. 2: Measured geometric dimensions of annular samples related to a nominal cross section of 5026.6 mm². True cross sections calculated from d_o and width.

Sample	d_i [mm]	d_o [mm]	Meas. Width [mm]	Cross Section (meas. width and d_o) [mm²]	Deviation to 5026.6 mm² [%]
Diameter		79.9		5014	-0.25
Annular 1	80.15	112.9	16.20	4921	-2.09
Annular 2	114.8	139.8	12.40	4963	-1.26
Annular 3	150	169.6	9.90	4967	-1.19
Annular 4	185	201.2	8.10	4914	-2.24
Annular 5	219.6	233.6	6.90	4912	-2.24
Annular 6	254.4	266.8	5.94	4868	-3.16

Later on and in order to compare the deformation for a constant aspect ratio of about three, different numbers of sheet layers were stacked for selected samples (Tab. 3). Since layers for two annular samples were laser cut in a second run, the dimensions differed slightly.

Tab. 3: Measured geometric dimensions of annular samples with an aspect ratio of approximately three. Cross section calculated using d_0 and material width. Deviation related to 5026.6 mm².

Preprints (www.preprints.org) | NOT PEER-REVIEWED | Posted: 29 February 2020 doi:10.20944/preprints202002.0457.v1

Sample	d_i [mm]	d_o [mm]	Meas. Width [mm]	Num-ber of Layers	Meas. Height [mm]	Cross Section [mm²]	Aspect Ratio	Deviation to 5026.6 mm² [%]
Annular 1	80.15	112.90	16.30	24	46.931	4947	2.88	-1.59
Annular 3	150	169.60	9.80	15	29.233	4920	2.98	-2.12
Annular 5	*219,6*	*233,60*	*6.9*	*10*	*19.521*	*4914*	*2.83*	*-2.24*
Annular 6	254.4	266.80	6.15	9	17.62	5036	2.87	+0.19

3 Experiments and Results

For all diffusion bonding experiments, additional baffle plates, made of TZM, were used, to protect the compression dies from damaging. These plates were coated by multiply spraying runs using alumina suspension and subsequent drying to prevent sticking at the samples at high temperatures. After placing the samples in the furnace, it was evacuated to a pressure smaller than 1*E-04 mbar. When reaching the criterion, the temperature was ramped up at a rate of 10 K/min for experiments performed in *furnace II* and 5 K/min in *furnace III*, used for larger formats (Tab. 4). The load was applied after reaching the set point of temperature within 5 min. All diffusion bonding experiments were performed at T= 1075°C, t= 4 h and p= 15 MPa. After diffusion bonding, the heating was turned off and the furnaces cooled down naturally according to their thermal mass.

3.1 Impact of Material Width on Deformation for Annular Test Samples of constant Height

Tab. 4 shows the measured heights of the samples consisting of ten layers, before and after diffusion bonding. Before diffusion bonding, the ten sheets were fixed using a pulsed laser for alignment reasons. Five spots for the height were measured (Fig. 1). For the round sample, the

Preprints (www.preprints.org) | NOT PEER-REVIEWED | Posted: 29 February 2020 doi:10.20944/preprints202002.0457.v1

heights were measured in all four directions as well as in the center. For cylindrical sample, heights were measured under an incremental angle of 72°. These values were averaged and deviations of flatness calculated (Tab. 4).

It turned out that the sheet thickness was approximately 1.95 mm only instead of 2.000 mm. The flatness deviation of all samples before diffusion bonding is generally less than 50 µm, but increases with increasing lateral dimensions. After diffusion bonding, the deviation of flatness increases considerably. Especially for smaller samples bonded in *furnace II*, the deviation of flatness increases steadily with lateral dimensions. The three largest annular samples, bonded in *furnace III*, show lower and nearly constant flatness deviations, due to a higher stiffness of the whole setup and the compression dies.

As a conclusion from Tab. 4, it was found, that the flatness deviation for experiments performed in *furnace II* increased for increasing sample diameters due to a low stiffness of the compression dies. Relating the deviation of flatness to the outer diameter, a constant value is obtained.

For *furnace III*, the deviation of flatness is nearly constant due to higher stiffness of this setup, independent of the sample diameter, leading to a decreasing flatness to diameter-ratio.

Furthermore, it can be seen that the impact of the flatness deviation on the accuracy of the deformation is much higher for *furnace II* compared to *furnace III*.

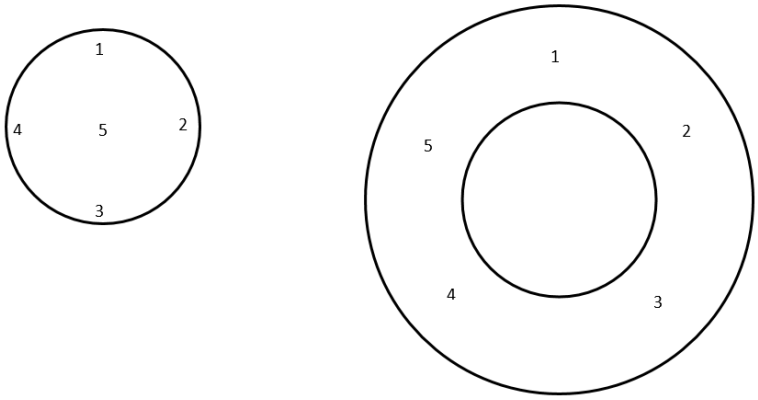

Fig. 1: Schematic representation of the height measuring points of the samples. Left: Round sample. Right: Circular sample

Preprints (www.preprints.org) | NOT PEER-REVIEWED | Posted: 29 February 2020 doi:10.20944/preprints202002.0457.v1

Tab. 4: Heights, deviation of flatness before and after diffusion bonding and deformation for samples made of ten layers.

Sample	Height before [mm]	Flate-ness Range [µm]	Height after [mm]	Flat-ness Range [µm]	Ratio Flatness to d_0 *10E-03	Defor-mation [mm]	Ratio Flatness to Defor-mation	Furnace
Diameter 80 mm	19.488	11	19.19	83	1.04	0.298	0.279	II (200 kN)
Annular 1	19.497	29	18.669	142	1.26	0.828	0.171	II
Annular 2	19.507	23	18.629	175	1.25	0.878	0.199	II
Annular 3	19.533	29	18.487	218	1.29	1.046	0.208	II
Annular 4	19.501	42	17.612	143	0.71	1.889	0.076	III (2 MN)
Annular 5	19.521	36	17.476	105	0.45	2.045	0.051	III
Annular 6	19.561	41	17.254	145	0.54	2.307	0.063	III

Tab. 5 displays the percentaged deformation of annular samples made of ten sheets each. It is obvious that the circular sample with d=80mm exhibits the greatest resistance to deformation. If the percentage deformation is related to the material widths, there is a strong increase for decreasing material cross-sections. However, as the height was constant, the aspect ratios were not constant but increasing. Therefore, the deformation related to the material width was also normalized to an aspect ratio of one.

Tab. 5: Percentaged deformation of samples related to material width and aspect ratio.

Sample	di [mm]	do [mm]	Meas. Width [mm]	Defor-mation [%]	Deformation per mm Mat. Width [%/mm]	Deformation per mm Mat. Width normalized to AR=1 [%/mm]	Aspect Ratio (AR)
Diameter		79.9		1.53	0.019	0.079	0.24

Preprints (www.preprints.org) | NOT PEER-REVIEWED | Posted: 29 February 2020 doi:10.20944/preprints202002.0457.v1

Annular 1	80.15	112.9	16.20	4.25	0.25	0.210	1.20
Annular 2	114.8	139.8	12.40	4.50	0.36	0.231	1.57
Annular 3	150	169.6	9.90	5.35	0.54	0.274	1.97
Annular 4	185	201.2	8.10	9.69	1.20	0.497	2.41
Annular 5	219.6	233.6	6.90	10.47	1.52	0.536	2.83
Annular 6	254.4	266.8	5.94	11.79	1.98	0.603	3.29

From Tab. 5, a huge impact of the bonding material width on deformation can be stated. The deformation covers a range of 1.53 % for the sample with a diameter of 80 mm to about the eight-fold of 11.79% for a material width of 5.94 mm only. For a material width of 16.2 mm, the deformation is more than the 2.5-fold than for a round sample 80 mm in diameter.

For a material width of 5.94 mm, what is about one third of 16.2 mm, the deformation triples, showing a roughly linear correlation between deformation and material width.

In general, it can be stated that the deformation and all related deformation values show a leap changing from *furnace II* to *furnace III*.

Fig. 2 shows the percentaged deformation versus the material width for the constant cross section of 5027 mm² and normalized to the material width in millimeters. For the cylindrical sample with a diameter of 80 mm a very small value of the normalized deformation of 0.02 %/mm is striking. For a material thickness of 16.2 mm, the normalized deformation increases to the twelvefold. If the material thickness decreases from 16.2 mm to 5.94 mm, it increases by the eightfold.

For the normalized deformation versus material width, a very good agreement with a potential function is obtained. It was found that the regression coefficient of the trend line drops if the deformation for the cylindrical samples was not taken into account. This affirms that the

Preprints (www.preprints.org) | NOT PEER-REVIEWED | Posted: 29 February 2020 doi:10.20944/preprints202002.0457.v1

deformation is described well by a potential function and for small material cross-sections, the deformation increases extremely strongly.

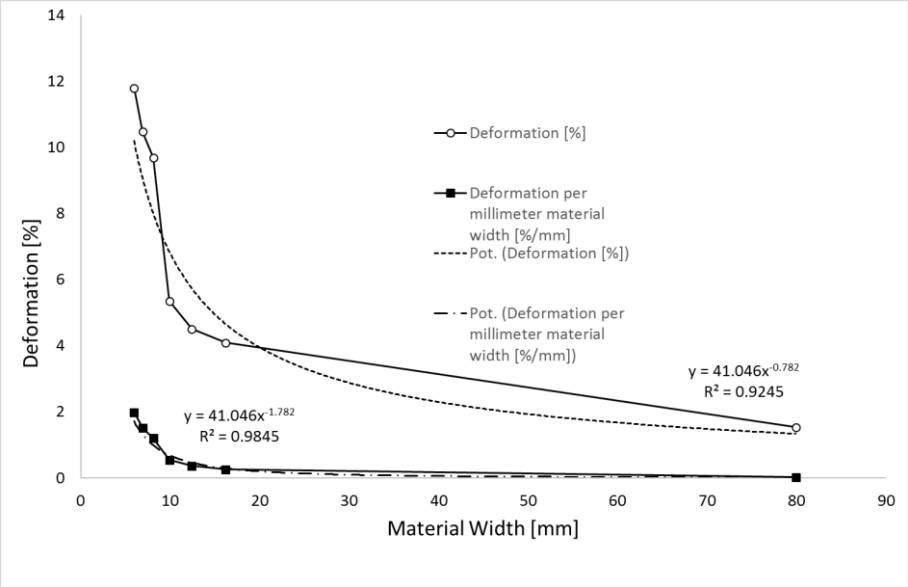

Fig. 2: Relation between material width and percentaged deformation at constant height.

For the diffusion bonding experiments, different deformation conditions have to be considered, because the round specimen can only be deformed to the outside. It was noticeable that the barrel-shaped distortion of the outline of annular specimens occurred only to the outside and not to the inside (Fig. 3). However, the inner contour did not correspond to that of the parallel-shifted, convex outer contour. Rather, vertical or even slightly convex areas are visible at the top and bottom. In the middle of the ring height, however, the contour is concave. It is concluded, that this is attributed to deformation obstruction due to friction on the compression dies during deformation.

Preprints (www.preprints.org) | NOT PEER-REVIEWED | Posted: 29 February 2020 doi:10.20944/preprints202002.0457.v1

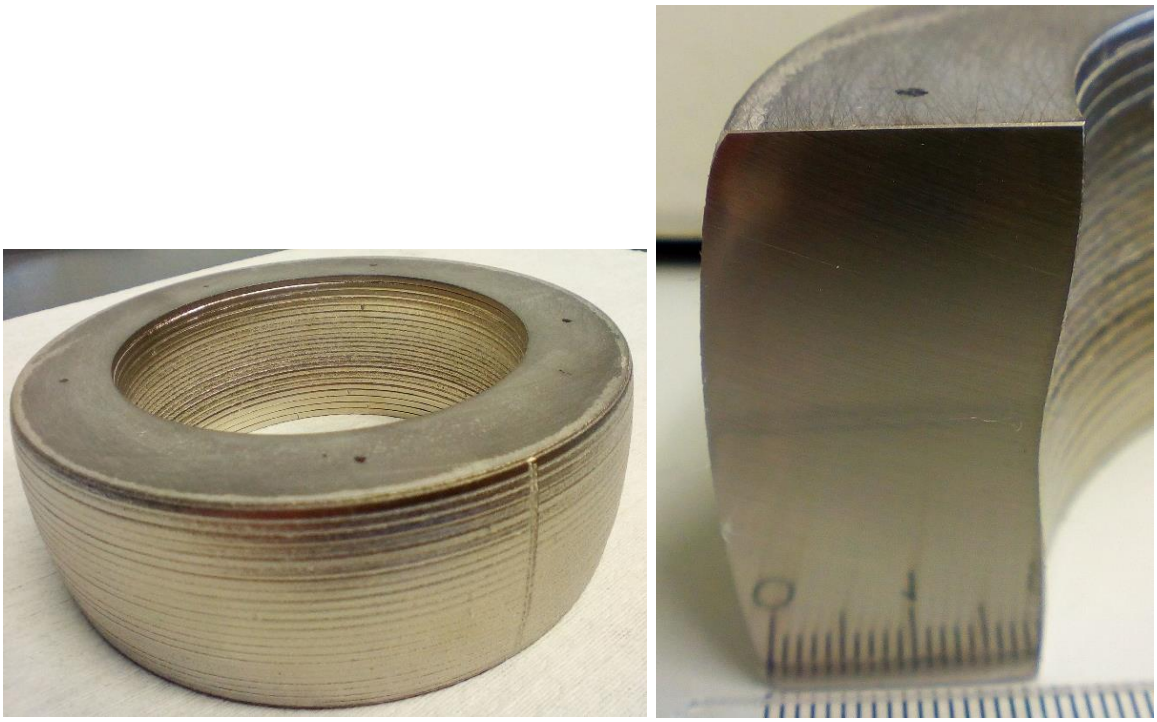

Fig. 3: Characteristic shape of distortion of annular samples. Left: Overview. Right: Cross section

Due to the lack of material data, e.g. elastic modulus, yield strength and tensile strength, for the austenitic stainless steel 1.4301 at the diffusion bonding temperature of 1075°C, the deformation behavior of the ring-shaped sample with an aspect ratio close to three at room temperature was simulated. For this, *ANSYS 2019 R1* was used. The simulation was carried out assuming an elastic-plastic material behavior, whereby the load level was adjusted in a way that the deformation obtained in the practical diffusion bonding experiment was achieved. Fig. 4 shows that the inner contour of the simulation of the deformation behavior of the annular sample corresponds qualitatively well with the observed profile of the diffusion-bonded sample in Fig. 3. It does not exactly follow a concave curvature. Rather, the sample is restricted in its deformation on the upper and lower side due to the mechanically very stiff compression dies and the friction that occurs in between. In contrast to the outer contour, the inner side is first vertical to convex before it changes to a concave curvature in the middle of the sample height.

Preprints (www.preprints.org) | NOT PEER-REVIEWED | Posted: 29 February 2020 doi:10.20944/preprints202002.0457.v1

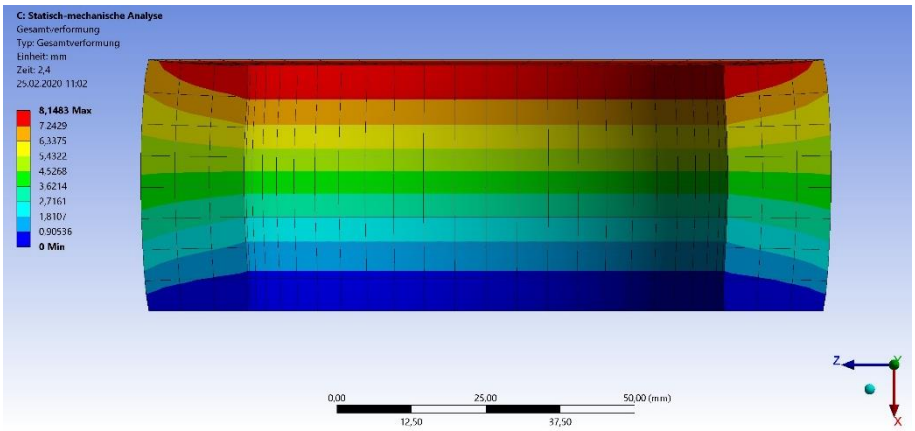

Fig. 4: Simulation of the qualitative deformation of a ring shaped sample of an aspect ratio close to three at room temperature.

3.2 Annular Samples with an Aspect Ratio of approximately three

For comparison reasons for diffusion bonding of samples with a constant aspect ratio of about three, to sample "*Annular 5"* of the first set of experiments, two additional samples were added, consisting of more layers (Tab. 5). Diffusion bonding samples were prepared by laser cutting as described in section 3.1

It was noticed that the deformation of the new samples of "*Annular 1*" and "*Annular 3*", with 24 and 15 layers to achieve an aspect ratio of approximately three, respectively, deviated strongly from the deformation of sample "*Annular 5*" of the first batch, which has an aspect ratio of about three, too.

Therefore, an additional experiment with the geometry of "*Annular 6*" and nine layers was performed. The deformation obtained from this last experiment fitted into the results of the other experiments at an aspect ratio of about three.

Tab. 6: Deformation of selected annular samples with an aspect ratio of three.

Sample	Height before [mm]	Height after [mm]	Flat-ness Range [µm]	Flatness related to Deformation [%]	Aspect Ratio	Defor-mation [%]	Deformation per Milli-meter Width [%/mm]

Preprints (www.preprints.org) | NOT PEER-REVIEWED | Posted: 29 February 2020 doi:10.20944/preprints202002.0457.v1

Annular 1 AR 3	46.931	39.0	240	3.03	2.88	16.9	1.04
Annular 3 AR 3	29.233	24.538	181	3.86	2.98	16.06	1.64
Annular 5	*19.521*	*17.476*	*105*	*5.13*	*2.83*	*10.47*	*1.52*
Annular 6 AR 3	17.62	14.547	143	4,65	2.87	17.44	2.84

Comparing the samples with an aspect ratio of about three, namely *Annular 1* and *3*, respectively, to *Annular 6* bonded the second batch, the deformation is nearly constant whereas the deformation normalized to the materials width steadily increases for decreasing material width (Fig. 5).

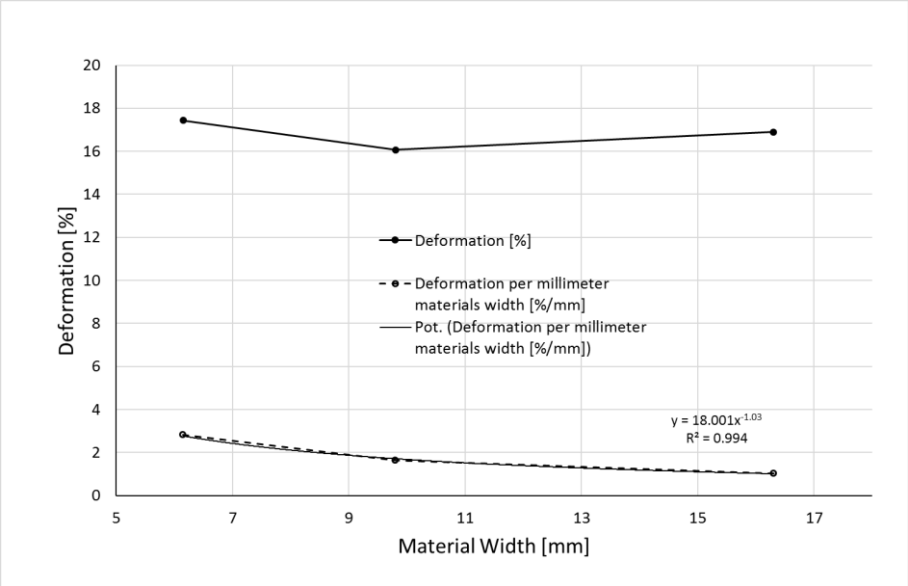

Fig. 5: Relation of deformation and related to the material width for Annular 1, 3 and 6, respectively with an aspect ratio of approximately three.

Comparing Tab. 6 to Tab. 5, it can be seen that the deformation for samples of a constant aspect ratio of three generally is much higher. For an aspect ratio of three, for *Annular 1* the deformation is fourfold compared to an aspect ratio of 1.20 from Tab. 5. For "*Annular 3"*, the deformation is tripled related to an aspect ratio of two.

Preprints (www.preprints.org) | NOT PEER-REVIEWED | Posted: 29 February 2020 doi:10.20944/preprints202002.0457.v1

3.3 Experiments to clarify the Discrepancy of the Deformation

However, when comparing the deformation of Annular 5 with the deformations of other samples with an aspect ratio of three in Tab. 6, it is obvious that the deformations do not show a linear dependence. The deformations obtained in different test series seem irregular.

As mentioned above, the first set of samples was made in one batch and the second batch of samples with an aspect ratio of about three were performed in a series of experiments later.

In between, in *furnace III* several runs were performed, including diffusion bonding of eight identical parts for an industrial partner possessing a completely different design and consisting of a few hundreds of layers. By comparing the deformation of these consecutively diffusion bonded parts, it was recognized that the deformation increased with the numbers of runs. The deformation of the last part was 1.5 % higher than for the first one (Tab. 7).

Tab. 7: Deformation of eight subsequently diffusion bonded parts of identical design.

Part-No.	Deformation [%]
1	2.82
2	3.15
3	3.8
4	3.56
5	3.93
6	3.96
7	4.36
8	4.33

Actually, diffusion bonding of the additional bonding experiment of *Annular 6* with an aspect ratio of three was performed 12 runs later than the diffusion bonding of "*Annular 5*" with ten sheet layers.

Preprints (www.preprints.org) | NOT PEER-REVIEWED | Posted: 29 February 2020 doi:10.20944/preprints202002.0457.v1

When searching for the causes for the diverging results, the authors also considered temperature measurement by means of thermocouples.

Contrary to widespread opinion, the thermoelectric voltage is not only generated at the contact point of the two thermoelectric wires made of different materials. Rather, additional thermoelectric voltages are generated along the profile of the temperature gradient. [6, 7]

The diffusion bonding process is performed under vacuum. Anyone who deals with diffusion bonding or heat treatment at high temperatures knows about debris in furnace chambers. Furthermore, it is generally known that chromium and its oxides in particular has a low vapor pressure. [8, 9] Also different metals may be subjected to evaporation depending on its content within a materials and their melting point. A few thermal cycling of *furnace III* after bonding the parts mentioned in Tab. 7, flaking of precipitations at the furnace wall was observed (Fig. 6, right). Flakes were characterized EDX using a microprobe *JEOL JXA 8530F*, equipped with an EDX-system *EX-94310F4L1Q* by *Jeol* with an energy resolution of 129 eV was used at a voltage of 15 keV and a current of 5.0 nA. The areas investigated and the results obtained are displayed in Fig. 7 and Tab. 8, respectively.

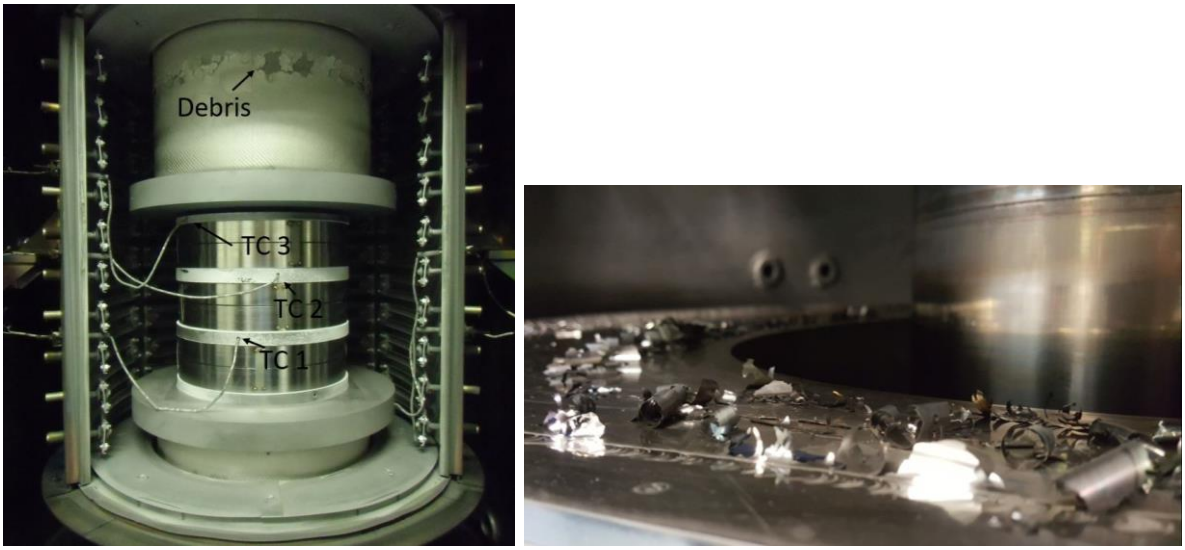

Fig. 6: Left: Diffusion bonding furnace with three sample thermocouples (TC) and debris. Right: Flaking precipitations at the cooled furnace wall.

Preprints (www.preprints.org) | NOT PEER-REVIEWED | Posted: 29 February 2020 doi:10.20944/preprints202002.0457.v1

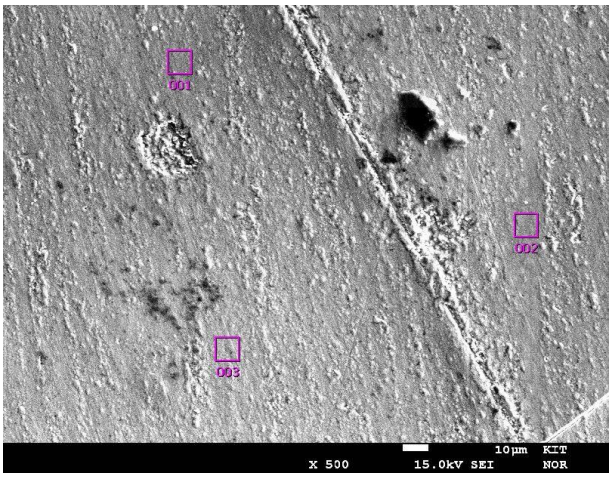

Fig. 7: **SEM of the flaking precipitations of the furnace (Fig. 6, right) with areas of interest.**

Tab. 8: **Composition of precipitation (Fig. 6, right), determined by EDX. Elements marked with * were manually added.**

Spot 1		Spot 2		Spot 3	
Element	**wt-%**	**Element**	**wt-%**	**Element**	**wt-%**
C*	1.16	C*	1.07	C*	1.07
O*	7.4	O*	7.04	O*	7.35
Na	2.47	Na	2.37	Na	2.52
Si*	0.24	Si*	0.28	Si*	0.27
S	0.95	S	0.95	S	0.93
Cr	3.67	Cr	3.53	Cr	3.48
Mn	64.97	Mn	65.24	Mn	65.11
Fe	7.51	Fe	7.37	Fe	7.4
Ni*	1.00	Ni*	1.12	Ni*	1.27
Cu	7.58	Cu	8.05	Cu	7.52
Sn	3.04	Sn	3.00	Sn	3.08
	99.99		**100.02**		**100.0**

Surprisingly, from Tab. 8, it can be seen that the precipitations consisted mainly of manganese, despite its content in austenitic stainless steel is specified to be below 2 wt-%. Since the melting point of manganese at 1246°C is the lowest of all alloying elements of stainless steel, obviously its partial pressure is highest. On the other hand, surprisingly, the content of chromium was rather low. The copper content is attributed to former diffusion bonding runs. If diffusion bonding, e.g. of copper, is carried out at significantly lower temperatures. Evaporated copper

Preprints (www.preprints.org) | NOT PEER-REVIEWED | Posted: 29 February 2020 doi:10.20944/preprints202002.0457.v1

migrates to the outside at subsequent diffusion bonding at higher temperatures in accordance with the temperature profile.

This observation means that the composition of thermocouple wires may change depending on the diffusion bonded metal and number of runs.

The individual thermocouple wires are isolated using 2-bore insulator pieces made of alumina for flexibility reasons. There is sufficiently space left in between for condensation of metal vapors. Despite their different positions, all three sample-thermocouples are normally within a temperature range of 5 K (Fig. 6, left).

In a first step, a *Pegasus 4853 Advanced* by *Isotech, UK*, supplied by *Klasmeier*, was used to check the thermocouples. The *Pegasus* was placed on an elevating platform in front of *furnace III* and the thermocouples were inserted into the calibrator block. It was started to three temperature setpoints at 1000, 1100 and 1200°C, respectively. It was found that the temperatures of the furnace thermocouples were between 300 to 400 K below the set points (!). In a next step, one thermocouple was replaced. Subsequently, a diffusion bonding test under vacuum at T = 1100°C for t= 1 h was carried out. New TC 1 was used for temperature control. It was found that old TC 2 was 23 to 29 K and TC 3 was 12 to 18 K below 1100°C. Furthermore, it can be seen from the curves, that the temperature of the old thermocouples is not constant but decreases with time (Fig. 8). In another publication evaluating the impact of bonding temperature on deformation, it was shown that a temperature raise of 20 K led to an increase in deformation of about 3%. [10]

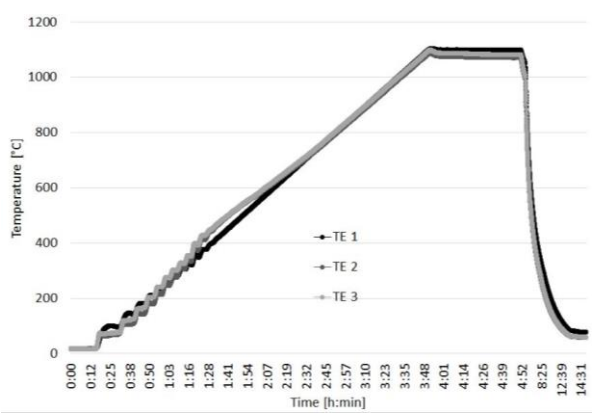

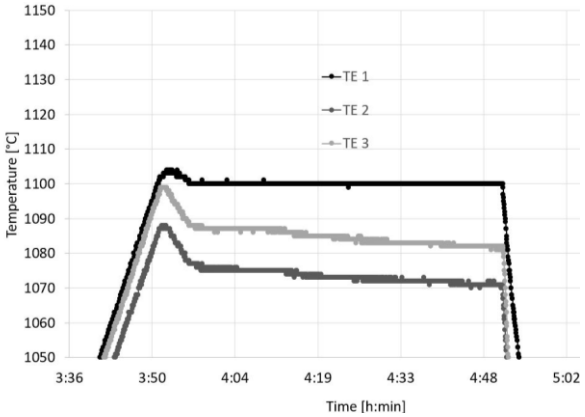

Preprints (www.preprints.org) | NOT PEER-REVIEWED | Posted: 29 February 2020 doi:10.20944/preprints202002.0457.v1

Fig. 8: Left: Temperature profile of diffusion bonding experiment with new TC 1 for comparison to old thermocouples. Right: Expanded detail at setpoint temperature of T= 1100°C.

For that reason, EDX-measurements were carried out on old cut-off TC 1. A microprobe *JEOL JXA 8530F*, equipped with an EDX-system *EX-94310F4L1Q* by *Jeol* with an energy resolution of 129 eV was used. At a voltage of 15 keV and a current of 3.2 nA, 2.500-3.000 counts per second were obtained. In Fig. 9, surfaces of the sensing tip, the platinum-wire and the Pt/10% rhodium-wire together with the measuring spots are displayed.

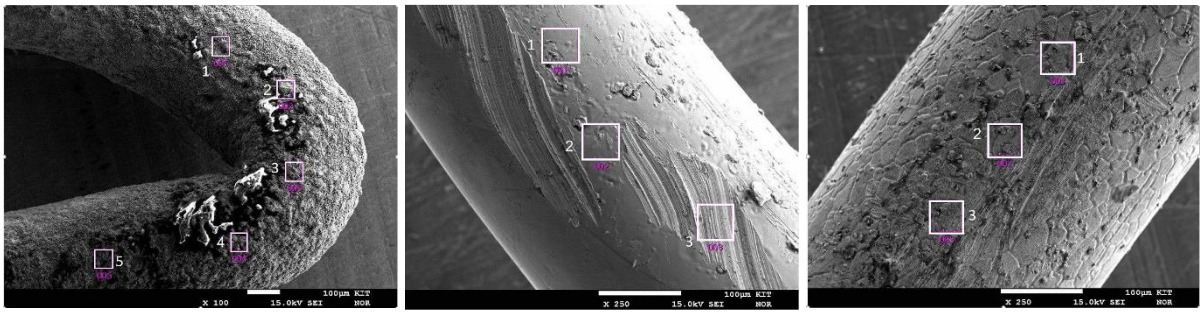

Fig. 9. EDX-measurements of thermoscouple tip (left), Pt-wire (middle), and Pt/10 Rh-wire (right)

In Tab. 9a-c, the results of EDX-measurements are summarized. For the tip of the TC (Fig. 9, left) it can be seen that spot 1 to 3 represent the Pt-wire. Spot 4 is in the transition range to the Pt/10%Rh-wire, whereas spot 5 represents the Pt/10%Rh-wire. Especially at the tip, large amounts of impurities by different metals such as iron, copper and chromium, are found due to diffusion and evaporation from the work pieces. Calcium and potassium may be attributed to skin excretions. For the Pt-wire less contaminants were found than for the Pt/10%Rh-wire. This might be attributed to the fact, that it is not clear, which spots of both wires in respect to the gaps between the alumina insulator pieces were investigated. For the Pt/10%Rh-wire, the Pt-Rh-ratio was found to be 10:1.

Tab. 9: EDX-measurements on tip, Pt- and Pt/10%Rh-wire of thermocouple, respectively. Chemical elements marked with * were added manually for analysis.

a) Tip of TC

Spot1	Spot 2	Spot 3	Spot 4	Spot 5

Preprints (www.preprints.org) | NOT PEER-REVIEWED | Posted: 29 February 2020 doi:10.20944/preprints202002.0457.v1

Element	wt-%	Element	wt-%	Element	wt-%	Element	wt-%	Element	wt-%
O*	17.44	O	20.33	O	21.57	O	20.16	O	22.03
Ca*	0.07	Mg	0.32	Mg*	0.15	Mg*	0.07	Al*	0.61
Cr	8.09	Al	1.45	Al*	0.72	Al	0.55	Si*	0.18
Mn*	0.91	K*	0.22	Si*	0.22	Si*	0.18	Ca*	0.41
Fe	7.59	Ca	1.61	K*	0.38	Ca	0.82	Cr	8.42
Cu	7.21	Cr	10.26	Ca	0.56	Ti	0.24	Mn*	2.64
Rh*	0.09	Mn*	1.38	Cr	8.69	Cr	5.86	Fe	11.33
Pt	58.60	Fe	10.1	Mn*	1.09	Mn*	1.09	Ni*	2.4
	100	Cu	7.99	Fe	8.93	Fe	7.81	Cu	7.14
		Rh*	0.12	Cu	5.71	Ni*	1.43	Rh	4.47
		Pt	46.22	Rh*	0.66	Cu	6.68	Pt	40.37
			100	Pt	51.31	Rh*	1.92		**100**
					99.99	Pt	53.19		
							100		

b) Pt-wire

Spot1		Spot 2		Spot 3	
Element	**wt-%**	**Element**	**wt-%**	**Element**	**wt-%**
Cu*	0.41	Cu*	0.43	Cu*	0.01
Rh	/	Rh	/	Rh	0.25
Pt	99.59	Pt	99.57	Pt	99.74
	100		**100**		**100**

c) Pt/Rh10-wire

Spot1		Spot 2		Spot 3	
Element	**wt-%**	**Element**	**wt-%**	**Element**	**wt-%**
O*	4.9	O*	5.59	O*	6.07
Cr*	1.03	Cr*	1.09	Cr*	0.81
Fe*	0.50	Fe*	0.28	Fe*	0.35
Ni*	0.28	Ni*	0.03	Ni*	0.47
Cu*	0.73	Cu*	0.97	Cu*	0.48
Rh	8.50	Rh	8.36	Rh	8.13
Pt	84.06	Pt	83.67	Pt	83.69
	100		**99.99**		**100**

Preprints (www.preprints.org) | NOT PEER-REVIEWED | Posted: 29 February 2020 doi:10.20944/preprints202002.0457.v1

4 Conclusions and Outlook

Systematic investigations on deformation as a function of material width showed that nominally constant joining temperature, contact pressure and bonding time may result in completely different percentaged deformations depending on the geometry of the components. Hence, it is difficult to estimate the expected deformation in advance for parts of arbitrary geometry.

It is emphasized, that additional impacts, e.g. alloying elements, formation of surface passivation layers or cold work hardening, may change diffusion behavior, formation of a monolithic bond and deformation considerably. Especially for different kinds of steel, depending on the type and quantity of alloying elements, primarily chromium and nickel, or others that behave like these two, the cubic face-centered or cubic space-centered structure may be stabilized. Both lattices have completely different packing densities, diffusion coefficients and thus deformation behavior of bonded devices.

The two batches of experiments underline the importance of temperature measurement and aging of thermos couples with time and during diffusion bonding processes.

This allows the following conclusions to be drawn:

- First, the temperature measurement using the *Pegasus* leads to completely different temperature values. Obviously, normal atmosphere and different temperature gradients along a thermocouple due to a varying measurement setup does not lead to comparable temperature measurement results.
- Second, the thermocouples are subject to aging. Since the thermoelectric voltage is not generated exclusively at the sensing tip, cutting off and reshaping the sensing tip before each bonding run does not ensure exact temperature measurement.
- Thirdly, since it is economically not feasible to replace the complete thermocouples after each run, the temperature measurement is always subject to uncertainty. For this

Preprints (www.preprints.org) | NOT PEER-REVIEWED | Posted: 29 February 2020 doi:10.20944/preprints202002.0457.v1

reason, it is not possible to predict reliably the deformation of new component designs based on the deformation obtained from previously diffusion bonded components.

- Fourthly, the deformation, as investigated in this paper and as described above, depends strongly on the component geometry.

Therefore, a generally applicable and reliable design of the diffusion bonding process itself, which guarantees a reproducibly successful diffusion bonding with limited deformation for parts containing complex mechanical microstructures, independent of the component design and accuracy of the temperature measurement, is important.

For this, there seem to be two possible ways:

- First, the constant contact pressure should be temporarily increased to a level where the flow rate of the material is high in order to level thickness tolerances and surface roughnesses of multilayered parts and enlarging the contact area at the atomic level. Due to a short dwell time, the deformation and the impact on the component are limited.
- Secondly, the possibility to define a maximum permissible absolute deformation per diffusion bonding program step as criteria to proceed to the next program step, in parallel to the specified dwell time. A prerequisite for this is that the component to be diffusion bonded has a minimum height due to limited distance measuring accuracy during the bonding process.

Thereby, it seems advantageous to select the constant contact pressure in a range where only a moderate strain rate of the material applies. The deformation of roughness peaks and the expansion of the contact area on the atomic scale, on the other hand, occurs predominantly during the short-term peak load. This increased contact pressure should be chosen two to three times as high. During the predominant duration of the overall dwell time at lower contact pressure, atomic diffusion takes place, closing pores at a considerably lower volume diffusion coefficient. This is also the difference to the procedure proposed in [11, 12]: The sole multiple

application of peak loads does not necessarily lead to the filling of remaining pore spaces. Instead, longer dwell times are required between peak loads.

Acknowledgments

The financial support from Helmholtz Program SCI (Storage and Cross-linked Infrastructure) is gratefully acknowledged.

References

[1] S. Jahn: „*Technologieentwicklung zur Herstellung variantenreicher innen-strukturierter Bauteile und Werkzeuge*“, PhD-thesis, TU Ilmenau, **2007**, p. 28f, 70f, ISBN: 978-3-86130-993-2

[2] DIN EN 10131, “Kaltgewalzte Flacherzeugnisse: Grenzabmaße und Formtoleranzen“, Tab. 1-4, **2006**

[3] T. Gietzelt, V. Toth, A. Huell, R. Dittmeyer, *Adv. Eng. Mater*., vol. 19, No. 2, online 31.10.2016, **2016**, doi: 10.1002/adem.201600344

[4] C. Zhang, H. Li, M. Q. Li, *Appl. Surf. Sci*., 371, **2016**, pp. 407-414, doi:10.1016/j.apsusc.2016.03.039

[5] T. Gietzelt, A. Hüll, V. Toth, F. Messerschmidt, R. Thelen, *Mat.-wiss. u. Werkstofftech*., vol. 49,**2018**, p. 185–192, doi:10.1002/mawe.201700154

[6] R. Pelster, R. Pieper, I. Hüttl, *PhyDid*, vol. 1, no. 4, **2005**, pp. 10-22, see under http://www.phydid.de/index.php/phydid/article/view/28, [Accessed: 2020-02-26]

[7] Klasmeier, Kalibrier- und Messtechnik GmbH, Fulda, see under http://www.temperaturblog.de/2015/07/29/thermospannung-entsteht-am-temperaturgradient, [Accessed: 2020-02-26]

[8] E. A. Gulbransen, K. F: Andrew, J. Eelctrochem. Soc., vol. 99, no. 10, 1952, pp. 402-406, doi: 10.1149/1.2779609

[9] Plansee SE, vapor pressure of chromium at selected temperatures, see under https://www.plansee.com/de/werkstoffe/chrom.html, [Accessed: 2020-02-26]

[10] T. Gietzelt, M. Walter, V. Toth, R. Dahm: „Impact of Bonding Temperature and Contact Pressure Regime on Deformation during Diffusion Bonding”, to be published in *metals*

[11] J. Aktaa, W. Basuki, P. Norajitra, L. Spatafora, Patent *DE 10 2012 1090782* A1, **2012**

[12] G. Sharma, D. K. Dwivedi, *Vacuum*, vol.. 146, **2017**, pp. 152-158